Neutron activation analysis of archeological artifacts using the ISIS pulsed neutron source

Cite as: AIP Advances 11, 075005 (2021); doi: 10.1063/5.0043935
Submitted: 12 January 2021 • Accepted: 8 June 2021 •
Published Online: 1 July 2021

Carlo Cazzaniga,[1,a)] Antonella Scherillo,[1] Anna Fedrigo,[1] Davide Raspino,[1] Francesco Grazzi,[2] and Christopher D. Frost[1]

AFFILIATIONS

[1] ISIS Facility, UKRI-STFC, Rutherford Appleton Laboratory, Didcot OX11 0QX, United Kingdom
[2] Consiglio Nazionale delle Ricerche, IFAC, Sesto Fiorentino, Italy

[a)] Author to whom correspondence should be addressed: carlo.cazzaniga@stfc.ac.uk

ABSTRACT

Archeological artifacts can be analyzed after neutron irradiation at the pulsed ISIS neutron and muon source, UK, using a newly installed high purity germanium gamma ray spectrometer to perform neutron activation analysis. In this work, the details of the measurement methods and data analysis are presented. In particular, it is explained how Monte Carlo calculations are necessary to evaluate the detection efficiency, taking into account self-shielding effects. The results for two certified bronze standards are presented. The good agreement between expected and measured compositions is promising for the use of this technique for archeological artifacts where the elemental concentration is often unknown. As an example, the analysis of a Chinese sword from the first or second century BC is presented.

I. INTRODUCTION

Neutron Activation Analysis (NAA) is a technique for determining the concentration of elements, which has been successfully used in many different applications including environmental measurements,[1–3] geology,[4,5] soil science,[6] nutritional epidemiology,[7] characterization of semiconductor materials,[8] and other high-purity materials.[9]

NAA is a non-destructive technique, which is very attractive for applications in archeometry[10,11] since it offers the possibility of quantitative bulk elemental analysis, contrary to other surface only techniques, such as XRF and ion beam analysis. Knowledge of the elemental composition, including major and trace elements, may provide clues on provenance (e.g., pigments[12] and metals[13]).

Despite the established method and very interesting successful examples,[14,15,18] NAA is not very widely used in archeometry. One of the main limitations is the availability of neutron sources for research, aggravated by the ending of operational life of several research reactors over the years.[16] In addition, even if high fluxes from reactors (which can be in the order of 10^{12}–10^{13} cm^{-2} s^{-1}; see, e.g., Ref. 10) can be used very effectively to detect elements in low concentrations (<ppm),[19] they are often not suitable for non-destructive measurements. In fact, the irradiation of an entire artifact with a high-flux neutron beam, where traditional NAA is available, can be problematic as the artifact activation would be too high both for the analysis and to return it to the museum within reasonable time. For this reason, often quantitative NAA is either not performed at all or performed in a destructive way, sampling the artifacts: samples need to be ground and prepared in capsules for irradiation to achieve the best accuracy. This makes it much less attractive for archeological samples. We intend to demonstrate a non-destructive method for quantitative NAA applied to large objects, which can be typically returned to the museums within weeks.

In this work, we present a new system for NAA at the pulsed ISIS neutron and muon source, UK,[20] where the irradiation was performed at the INES beamline.[21] The thermal neutron flux on a water moderated beamline, such as INES, is of the order of 10^6 cm^{-2} s^{-1}, which is much more suitable as the risk of activation is lower. This paper will focus on the investigation of metallic samples as a case study for demonstrating the new NAA apparatus.

The main advantage of this new setup is that it becomes complementary to other techniques that are used on the same beamline for materials science, such as Time of Flight Neutron Diffraction (ToF-ND),[17] Neutron Resonance Capture Analysis (NRCA),[22] and Neutron Resonance Transmission Imaging (NRTI).[23] ToF-ND

investigates the properties of the material, allowing for the quantification of the crystalline phases in the sample and for the microstructural analysis, such as crystallite size, texture, and residual strain determination. NRCA is a time of flight technique based on the detection of a prompt gamma ray from a nucleus in the samples after absorption of a neutron of energy corresponding to a resonance.[24] It is a successful technique for the semi-quantitative determination of the elemental composition of materials. This is particularly useful in metals for identifying alloying elements and many trace elements. NRTI is a radiographic technique, which allows for an enhanced detection of certain elements and isotopes in the material investigated, achieving 2D and possibly 3D elemental mapping through transmission measurements.[23] All these techniques use the pulsed nature of the neutron source, as they exploit the time of flight method to measure the neutron energy.

Moreover, NRCA and NRTI have limitations in measuring the concentration of trace elements in the material due to the present quality of the data and the need to go toward very short time of flight values where the gamma burst of the spallation phenomenon is still very intense. Therefore, it is of great importance to add NAA as the complementary method to the available techniques. It should be noted that NAA is not sensitive to every element; a few elements, such as Li, Be, C, S, and Pb,[25] cannot be detected. On the other hand, some elements, e.g., Mn, As, Br, Ag, In, and Au, can be detected in extremely low concentrations (parts per million or better).

The prompt gamma emission techniques, such as NRCA, offer advantage in the detection of elements that decay too rapidly to be measured by NAA, elements that produce only stable isotopes, or elements with weak decay gamma-ray intensities. NAA is better suited for the detection of long-lived radionuclides that suffer from interference by shorter-lived radionuclides since there is a great degree of flexibility in the time span before between the activation of the sample and the start of the gamma-ray measurements.

It is also important to underline that the addition of NAA to the set of measurements does not require extra beam time after the sample has been irradiated during the other measurements since NAA is performed post-irradiation.

II. EXPERIMENTAL

A. The neutron beam

Neutron irradiation of samples was performed at the INES beamline,[21] a general purpose neutron diffractometer. At ISIS, neutrons are produced by spallation reaction of 800 MeV protons hitting a tungsten target. In the case of INES, the neutrons are moderated to energy more suitable for diffraction by a water moderator at about 25 °C to obtain a thermal spectrum (0.01–0.5 eV). This spectrum, however, maintains a quite relevant epithermal component (0.5 eV–500 keV) and is therefore different from the thermal spectrum from a fission reactor.[26] The detailed shape of the spectrum needs to be taken into account in the data analysis. The spectrum presented in Fig. 1 was measured with the time of flight technique by the same position sensitive n-GEM neutron detector used for NRTI.[23] The thermal neutron flux on INES is about $2.12 \cdot 10^6$ cm^{-2} s^{-1} for the accelerator operating at 170 μA.

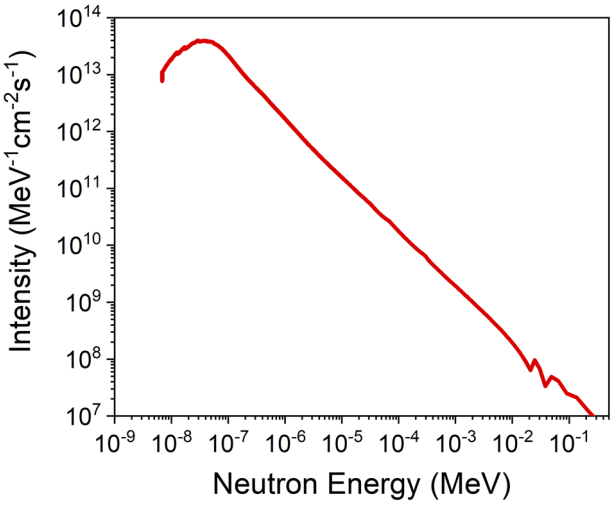

FIG. 1. The neutron spectrum of the INES beamline used for irradiation measured with a position sensitive n-GEM based neutron detector.

B. The gamma ray spectrometer

Gamma ray spectroscopy is performed after neutron irradiation using a newly installed High Purity Germanium (HPGe) detector. This is a coaxial detector system of the F-profile series by ORTEC.[27] The detector is cooled using liquid nitrogen and is contained in a low background lead shielding. The system uses a traditional analog chain with a preamplifier (model A257P), a spectroscopy amplifier (model 671), and a multichannel analyzer (EASY-MCA). The detector is biased with positive 2.1 kV.

The HPGe detector is calibrated in energy and efficiency using certified laboratory γ-ray sources of ^{241}Am, ^{137}Cs, ^{133}Ba, ^{54}Mn, and ^{60}Co giving known γ-lines. These are point-like sources sealed in plastic coins placed at the measurement position "H1" at a distance of 5 cm from the HPGe crystal. The efficiency of the detector $\varepsilon_{\text{point}}$ is defined as the number of counts in the full-energy peak divided by the number of emitted γ-rays at the source.

A model of the germanium detector is then built with the Monte Carlo radiation transport code MCNP6.[28] The simulated efficiency for a point-like source can be benchmarked by the measurements as presented in Fig. 2. It is interesting to notice the quite strong dependence of the efficiency as a function of the γ-ray energy (E_γ). Lower energies (E_γ < 100 keV) are cut by the aluminum window (1 mm), dead layer (0.7 mm—part of Ge volume that is not active for detection), and plastic support. E_γ > 100 keV can penetrate easily the dead layers, and the decreasing behavior is given by the probability of interaction with the HPGe crystal. The good agreement between measurements and simulation gives confidence in the model that can then be used to simulate an object with complex extended geometry.

C. The samples

In this work, we irradiated two copper-based standards to demonstrate the capability of the setup for quantitative measurements of elements in metallic artifacts. The first standard is a leaded

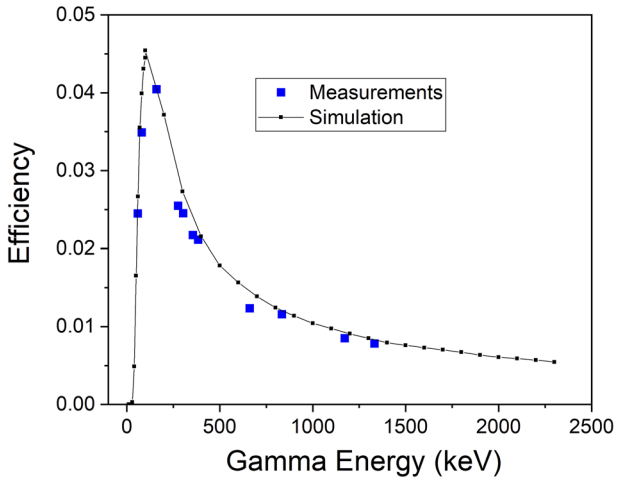

FIG. 2. Measured and simulated efficiency ε_{point} of the new HPGe system for a point-like source at the sample position.

bronze (chill cast) with 8.26% Sn, 12.46% Pb, and other elements in traces certified by MBH ANALYTICAL LIMITED.[29] This is a disk of 40 mm diameter and 16 mm height. The second standard is a brass with 0.45% Sn, 5% Zn, and other elements in traces certified by TECHLAB.[30] This is a disk of 40 mm diameter and 15 mm height. Certifications are based on analytical work carried out by laboratories with proven competence in accordance with ISO standards. Irradiation time was 5935 and 2899 s, respectively. Wait time, between irradiation and the start of gamma spectroscopy, was 591 and 734 s, respectively.

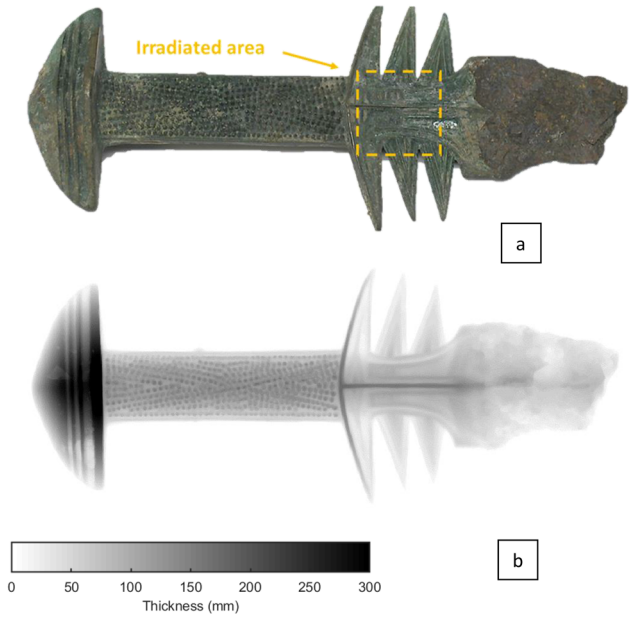

FIG. 3. (a) Picture of the artifact under investigation, a bimetallic Chinese sword likely from the first or second century BCE. (b) Thickness map of the sword fragment calculated from 3D tomographic data.

As a case study of a sample of archeological interest, we irradiated a sword fragment (Fig. 3) that resembles a published example with a similar hilt[31] labeled as originating from burials in the mountainous regions of Longpaozhai, in the Min River Valley in Sichuan, China, dating from the second or first century BCE. It has an iron blade mounted on a bronze hilt, and as it can be seen in the picture, the bronze hilt is very well preserved in contrast to the blade. Bimetallic swords have been found in many parts of Central China, with the earliest example dating as early as the Shang dynasty (1600–1100 BCE). The sample has been also analyzed using the INES beamline complementary capabilities, ToF-ND and NRTI.[23] We irradiated the hilt on its flattest part with a 4×4 cm^2 beam (see the yellow dashed square in Fig. 3). Here, the artifact is about 0.8 mm thick [see Fig. 3(b)]. Irradiation time and wait time were 2100 and 540 s, respectively. Measurement times on the gamma spectrometer are of increasing length, ranging from 10 min to 24 h, in order to better discriminate different half-lives.

III. DATA ANALYSIS

A. Calculation of an element's mass

It is assumed that the reader is already familiar with the theory of radioactive decay that can be found in the literature and books, e.g., Ref. 32. In a nutshell, the goal is to calculate the mass m (g) of a given element in a sample, measuring the number of counts (n_{count}) in characteristic peaks of the gamma spectra given by the decay of a radioisotope produced by the neutron activation of a stable isotope. From the theory, it is possible to derive the following formula:

$$m = \frac{n_{count}}{\varepsilon \cdot R} \frac{\lambda}{\left(1 - e^{-\lambda t_{irr}}\right) e^{-\lambda t_{wait}} \left(1 - e^{-\lambda t_{meas}}\right)} \frac{M}{N_{av} \cdot \theta \cdot I_g}. \quad (1)$$

The following quantities are found in the literature and databases (e.g., Ref. 33):

- M is the molar mass (g/mol).
- θ is the isotopic fraction of the stable isotope.
- N_{av} is the Avogadro number ($6.022 \cdot 10^{23}$ mol^{-1}).
- λ is the decay constant of the radioisotope (s^{-1}), also given by $\lambda = \frac{\ln(2)}{HalfLife}$.
- I_g is the probability that a decay of the radioisotope will emit a γ-ray of a specific energy.

The following quantities are measured during the experiment:

- t_{irr} is the irradiation time (s).
- t_{wait} is the time elapsed from the end of irradiation and the start of the gamma spectroscopy measurement (s).
- t_{meas} is the measurement time of gamma spectroscopy (s).

Multiple gamma spectroscopy measurements are taken in a separate time series after the irradiation of a sample with both increasing t_{wait} and t_{meas}. Doing so, one can measure first the short lived isotopes, which quickly decay away, and have cleaner measurements for long lived isotopes.

In the next two paragraphs, it is explained how more effort is needed to evaluate ε, the efficiency of detection of a γ-ray of known E_γ, and the activation rate R (s^{-1}) in a given neutron field.

B. Correction factor for the efficiency

It has been shown in Sec. II B how ε is strongly dependent on E_γ for the simple case of a point-like source (ε_{point}). For the case of a point-like sample, the experimental curve obtained with calibration sources would be sufficient. However, Monte Carlo simulations are needed to evaluate the efficiency for a macroscopic object. There are two effects that come into play: (a) the geometric effect, which is the fact that the source is extended in space; and (b) the sample self-shielding effect, which is the fact that γ-rays will be attenuated by the materials of the sample. Both effects will reduce ε overall, but the second effect will be much stronger at lower energies, and this effect is particularly enhanced for a metallic object because of its high density and high Z. The results of the simulations for both the standard disk and the sword are presented in Fig. 4, where the correction factor K (E_γ) is such that $\varepsilon(E_\gamma) = K(E_\gamma)\varepsilon_{point}(E_\gamma)$. The simulated sword was assumed to be containing only the main elements: copper with a core of iron. The disks are perfect cylinders containing only the main elements (copper and lead and copper and zinc, respectively) following the composition specifications as certified.

An important contribution to the correction factor in the case of the sword comes from the fact that it was not possible to place the artifact with the irradiated part on the axis of the detector. Therefore, the source was on average at a greater distance from the HPGe detector, and this accounts for the lower efficiency as can be appreciated in Fig. 4.

C. Correction of the activation rate

The activation rate per nucleus R (s^{-1}) of a given isotope is given by the following convolution of the nuclear cross section $\sigma(E_n)$ (cm^2) of the relevant reaction [(n,γ) in this case] and the neutron

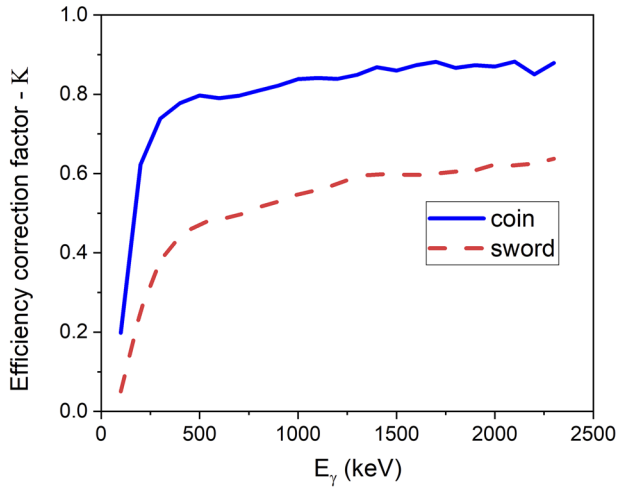

FIG. 4. Results of the simulations for the correction factor to the efficiency of a disk and a sword shaped source calculated with MCNP as a function of the γ-ray energy.

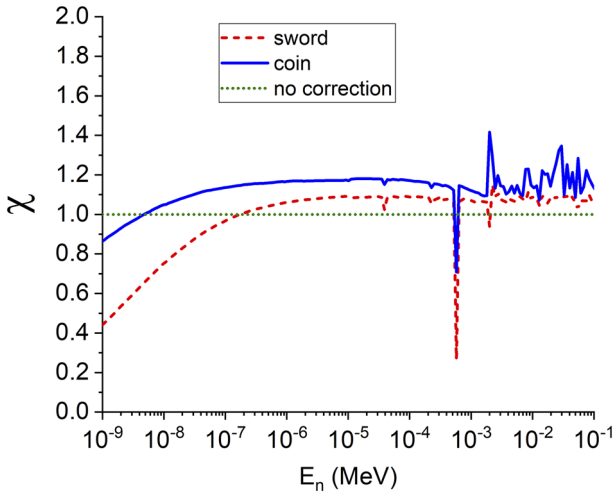

FIG. 5. Correction factor to the neutron flux as a function of energy due to the presence of the sample.

differential flux φ (E_n) (MeV^{-1} s^{-1} cm^{-2}):

$$R = \int \sigma(E_n)\varphi(E_n)dE_n. \quad (2)$$

Nuclear cross sections can be easily found in nuclear data libraries.[34]

The incoming neutron flux $\varphi_0(E_n)$ is presented in Fig. 1. However, a correction to R is needed due to the fact that the sample itself modifies the neutron spectrum across its thickness. Again, we used MCNP to evaluate this effect with Monte Carlo simulations. We simulate the average neutron flux in the sample volume as a function of energy and calculate a flux correction factor $\chi(E_n)$, presented in Fig. 5 for the cases under study, such that $\varphi(E_n) = \chi(E_n)\varphi_0(E_n)$. It is interesting to see that, for low energy and for resonance energy, the effect is a self-attenuation of the flux ($\chi < 1$), as neutron capture is dominant. For intermediate epithermal energy, we observe $\chi > 1$, meaning that there is a slight enhancement of the flux due to neutron scattering (the scattered neutron would have longer paths and be reflected back into the sample). This effect of increased reduction of lower energies as the beam travels further into the material is the so-called "beam hardening." However, we also need to notice that this effect is a relatively small correction, as overall $\chi \approx 1$ for samples of this size (≈cm thick).

IV. RESULTS

Characteristic γ-ray lines have been identified in the measured spectra. In Fig. 6, we show as an example a γ-ray spectrum measured for the sword case and a zoom on the characteristic peak of ^{76}As. Here, the reader can assess the good quality of the data. The peaks have good energy resolution (in the example, the peak centered at 559.1 keV has a resolution of 0.2% FWHM) and are well fitted by a Gaussian distribution.

The results for the two copper-based standard samples are presented in Fig. 7 and Table I, compared to the expected elemental concentrations. It is very promising to notice a rather good overall

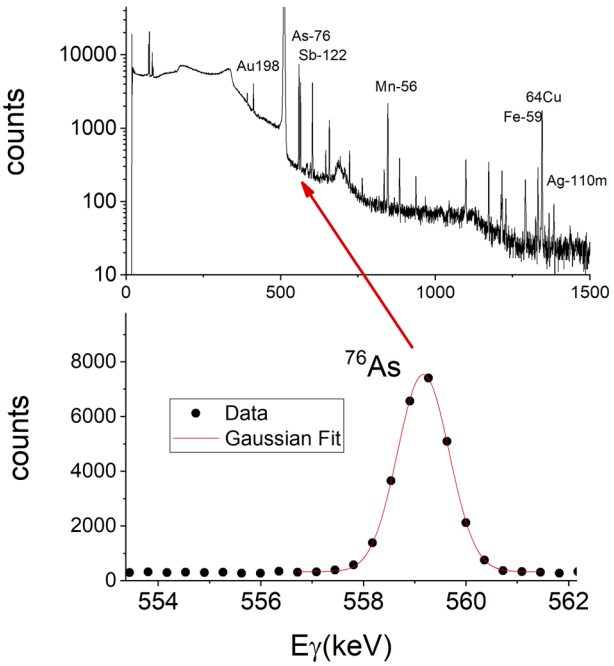

FIG. 6. Example of a γ-ray spectrum of the sword measured with the HPGe detector (top) and a zoom on the full-energy peak of ^{76}As (bottom).

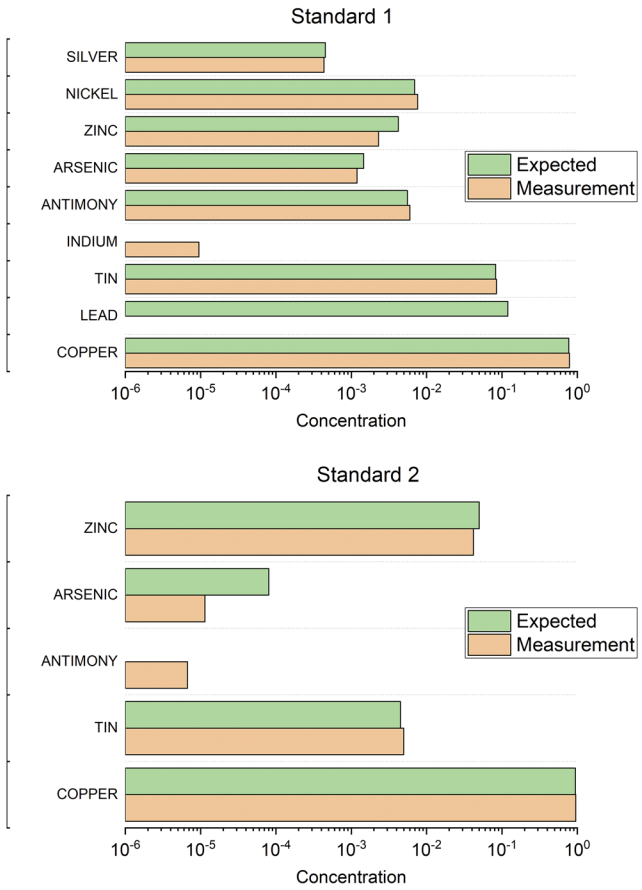

FIG. 7. Results for the two copper-based standards. Measured and expected concentration values are compared.

agreement (discrepancies <10%) and that this agreement holds over several different orders of magnitude of concentration.

To evaluate the uncertainties, the following major contributions are considered: (a) an uncertainty of 10% on the flux characterization and monitoring, as it is reported in Ref. 35 for the detector used; (b) an uncertainty of 8% on the evaluation of the detector efficiency, which includes the use of Monte Carlo simulations, as from the study reported in Fig. 2; and (c) a typical statistical uncertainty of 5% for counting statistics, even if this can vary from element to element. The combination gives an uncertainty of about 14%, which is similar of what is estimated in foil activation studies.[36] However, other systematic uncertainties can be present in some cases, for example, when the geometry of the sample is not well known or not well represented in the simulation.

TABLE I. Numerical value of the results of the concentration of elements for the two copper-based standards, also represented graphically in Fig. 7.

Standard 1			Standard 2		
Element	Measured	Expected	Element	Measured	Expected
Copper	0.79 ± 0.01	0.7723	Copper	0.95 ± 0.01	0.944
Lead	N/A	0.12	Tin	$(4.9 \pm 0.68) \cdot 10^{-3}$	$4.5 \cdot 10^{-3}$
Tin	$(8.4 \pm 1.2) \cdot 10^{-2}$	$8.26 \cdot 10^{-2}$	Antimony	$(6.6 \pm 0.92) \cdot 10^{-6}$	$<10^{-5}$
Indium	$(9.5 \pm 1.3) \cdot 10^{-6}$	N/A	Arsenic	$(1.14 \pm 0.15) \cdot 10^{-5}$	$8 \cdot 10^{-5}$
Antimony	$(6.0 \pm 0.84) \cdot 10^{-3}$	$5.57 \cdot 10^{-3}$	Zinc	$(4.19 \pm 0.58) \cdot 10^{-2}$	$4.99 \cdot 10^{-2}$
Arsenic	$(1.19 \pm 0.16) \cdot 10^{-3}$	$1.46 \cdot 10^{-3}$			
Zinc	$(2.3 \pm 0.7) \cdot 10^{-3}$	$4.2 \cdot 10^{-3}$			
Nickel	$(7.6 \pm 1.1) \cdot 10^{-3}$	$6.9 \cdot 10^{-3}$			
Silver	$(4.3 \pm 0.6) \cdot 10^{-4}$	$4.5 \cdot 10^{-4}$			

The following points are also worth to be discussed:

- Zinc presents larger discrepancies with respect to other elements (about 45% for standard 1 and about 16% for standard 2). We note that the measurement of the zinc content is based on the partial reaction $^{68}Zn(n,\gamma)^{69m}Zn$, leading to a metastable state. We find in the literature that larger than usual discrepancies between measurements and tabulated nuclear data are reported for this reaction (e.g., a discrepancy of 25% is reported in Ref. 37).
- In standard 1, there is a lead concentration that cannot be measured. In fact, it is not possible to measure lead using NAA with thermal neutrons because all the capture reactions give stable isotopes.
- Indium and antimony have been measured in standard 1 and standard 2 but were not expected from the data sheet. This is because the concentration is very low, in the order of 10^{-5} (10 ppm), and elements in such a low concentration were not reported in the data sheets. NAA is very sensitive to both indium and antimony, thanks to their high absorption cross sections.

In Fig. 8 and Table II, the results for the Chinese sword are presented. It is interesting to discuss these results in correlation with ToF-ND and NRTI measurements that have been presented in Ref. 23. The following considerations can be made:

- NAA provides quantitative results for elements in low concentrations that are not easy to obtain by the other techniques. All the elements that were found with NRTI are also identified with NAA in the same sample. NRTI can give a map of the element concentration, but there are difficulties in extracting accurate quantitative information as explained in the Introduction.
- From an archeometric point of view, the characterization of the alloy in terms of its main elements, Cu and Sn in this case, is very useful to assess changes in production technology, access to tin and other metals, consistency in alloying different materials, etc.[38] This is done very effectively with ToF-ND when dealing with substitutional alloys, such as brasses and bronzes,[38] but it does not apply for carbon steels where the alloy is interstitial. ToF-ND data were analyzed using a Le Bail fit,[38] highlighting dendritic structures with an average 10.5 ± 0.5 wt. % Sn for the area irradiated for NAA. Dendritic segregation is a common microstructure that arises during casting and cooling of impure metals or deliberate alloys. Dendrites form as one of the constituents of the melt that has a different melting point than the other: in the case of bronze, Cu melts at 1083 °C and Sn at 232 °C. As the alloy cools, a compositional gradient forms from the inner region of a dendritic arm to the outer surface.
- NAA allowed us to evaluate the tin concentration in the bronze (8 ± 1 wt. %). The difference can be acceptable in many cases, but it is more then what we expected from the analysis of the standards. It is probably due to a combination of different causes: (a) the approximations done with MCNP simulations regarding the geometry and composition of the matrix (the sword is approximated by simple flat geometry), (b) possible errors in evaluating the positioning of the sample with respect to the HPGe detector, (c) previous irradiations of the same object possibly not well taken into account, and (d) the assumption in the estimation of the Sn content from diffraction data that the alloy is binary. However, despite the limitation and possible discrepancies in the order of 20%, it was a confirmation of the suitability of NAA to determine with reasonable accuracy the elemental concentration of a complex artifact such as the one under investigation. In this case, it was also possible to determine the presence of As in the alloy. Although arsenical bronze has been known since the early bronze age, it is still not entirely clear to what extent arsenic was deliberately added to copper for its silvery sheen or to improve some mechanical characteristics of the alloy, considering that arsenic is also present in a number of copper containing ores. Therefore, some natural contamination of the copper with arsenic would have been unavoidable. It is, therefore, important to quantify the content of As in bronzes to help addressing this issue.
- It is very relevant to notice that with NAA, it is possible to measure elements in low concentrations (silver, antimony, gold, and arsenic in such a low amount that does not affect the copper alloy lattice parameter) that cannot be measured

TABLE II. Measured concentration of elements for the archeological artifact under test, also represented graphically in Fig. 8. Details about ND results and NRTI maps are available in Ref. 23.

Element	Measured with NAA	Measured with ND	Detected in NRTI maps
Tin	0.08 ± 0.011	0.10 ± 0.005	Yes
Indium	$(5.9 \pm 0.83) \cdot 10^{-6}$	···	Yes
Antimony	$(2.5 \pm 0.35) \cdot 10^{-3}$	···	Yes
Arsenic	$(3.3 \pm 0.46) \cdot 10^{-3}$	···	Yes
Silver	$(1.6 \pm 0.22) \cdot 10^{-2}$	···	Yes
Gold	$(9.1 \pm 1.3) \cdot 10^{-5}$	···	Yes

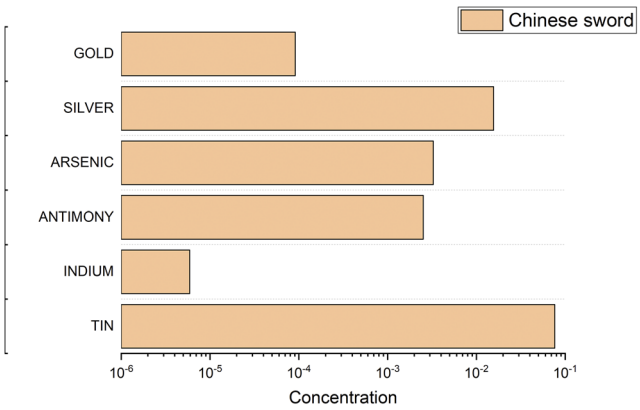

FIG. 8. Results for the archeological artifact under test.

with ToF-ND but only with NRCA or NRTI. The presence of silver and gold is interesting from an archeological point of view, as it may suggest that some decorations, which are no longer visible, might have been present on the object.

V. CONCLUSIONS

NAA has been used successfully to characterize non-destructively metallic artifacts after irradiation on the INES beamline at the ISIS neutron and muon source. The measurements of copper-based standard samples give confidence in the quantitative results of this powerful method of analysis. The method can then be applied not only to artifacts of archeological interest but also to geological samples and, more generally, where elemental quantification is required.

The main advantage of the development of this new setup for analysis at ISIS is the possibility of integration with complementary methods, such as ToF-ND, NRCA, and NRTI. All these techniques combined give the possibility for non-destructive bulk testing of extended samples of complex geometry, such as, but not only, objects of cultural heritage interest.

DATA AVAILABILITY

Raw data were generated at the ISIS large scale facility. Derived data that support the findings of this study are available from the corresponding author upon reasonable request.

REFERENCES

[1] R. Dams, J. A. Robbins, K. A. Rahn, and J. W. Winchester, "Nondestructive neutron activation analysis of air pollution particulates," Anal. Chem. **42**(8), 861–867 (1970).

[2] K. K. S. Pillay, C. C. Thomas, J. A. Sondel, and C. M. Hyche, "Determination of mercury in biological and environmental samples by neutron activation analysis," Anal. Chem. **43**(11), 1419–1425 (1971).

[3] M. Gallorini, R. R. Greenberg, and T. E. Gills, "Simultaneous determination of arsenic, antimony, cadmium, chromium, copper, and selenium in environmental material by radiochemical neutron activation analysis," Anal. Chem. **50**(11), 1479–1481 (1978).

[4] P. J. Potts, O. Williams Thorpe, M. C. Isaacs, and D. W. Wright, "High-precision instrumental neutron-activation analysis of geological samples employing simultaneous counting with both planar and coaxial detectors," Chem. Geol. **48**(1-4), 145–155 (1985).

[5] I. L. Gibson and P. Jagam, "Instrumental neutron activation analysis of rocks and minerals," in *Neutron Activation Analysis in the Geosciences* (International Nuclear Information System, 1980), Vol. 13, p. 13680075.

[6] R. D. Koons and P. A. Helmke, "Neutron activation analysis of standard soils 1," Soil Sci. Soc. Am. J. **42**(2), 237–240 (1978).

[7] T. Nichols, J. Morris, M. Mason, V. Spate, C. Baskett, T. Cheng, C. Tharp *et al.*, "The study of human nails as an intake monitor for arsenic using neutron activation analysis," J. Radioanal. Nucl. Chem. **236**(1-2), 51–57 (1998).

[8] K. Fujinaga and K. Kudo, "Instrumental neutron activation analysis of semiconductor grade silicon," J. Radioanal. Chem. **52**(2), 411–419 (1979).

[9] W. J. Ross, "Activation analysis of high purity materials," Anal. Chem. **36**(6), 1114–1119 (1964).

[10] M. D. Glascock and H. Neff, "Neutron activation analysis and provenance research in archaeology," Meas. Sci. Technol. **14**(9), 1516 (2003).

[11] R. J. Speakman and M. D. Glascock, "Acknowledging fifty years of neutron activation analysis in archaeology," Archaeometry **49**(2), 179–183 (2007).

[12] J. Zöldföldi and Zs. Kasztovsky, "Provenance study of lapis lazuli by non-destructive prompt gamma activation analysis," in *Proceedings of the 7th International Conference of Association for the Study of Marble and Other Stones in Antiquity, BCH Suppl*, edited by Y. Maniatis (Bulletin de Correspondance Hellenique, 2009), Vol. 51, pp. 677–691.

[13] A. M. Pollard, *Beyond Provenance: New Approaches to Interpreting the Chemistry of Archaeological Copper Alloys* (Leuven University Press, 2018).

[14] R. L. Bishop and M. James Blackman, "Instrumental neutron activation analysis of archaeological ceramics: Scale and interpretation," Acc. Chem. Res. **35**(8), 603–610 (2002).

[15] M. I. Dias and M. I. Prudêncio, "Neutron activation analysis of archaeological materials: An overview of the ITN NAA laboratory, Portugal," Archaeometry **49**(2), 383–393 (2007).

[16] A. Aspinall, S. W. Feather, and C. Renfrew, "Neutron activation analysis of Aegean obsidians," Nature **237**(5354), 333–334 (1972).

[17] F. Grazzi, L. Bartoli, S. Siano, and M. Zoppi, "Characterization of copper alloys of archaeometallurgical interest using neutron diffraction: A systematic calibration study," Anal. Bioanal. Chem. **397**(6), 2501–2511 (2010).

[18] H. Postma and P. Schillebeeckx, "Neutron resonance capture and transmission analysis," in *Encyclopedia of Analytical Chemistry: Applications, Theory, and Instrumentation* (Wiley Online Library, 2006).

[19] K. Soliman and L. Zikovsky, "Determination of Br, Ca, Cl, Co, Cu, I, K, Mg, Mn, Na, Rb, S, Ti and V in cereals, oils, sweeteners and vegetables sold in Canada by neutron activation analysis," J. Food Compos. Anal. **12**(2), 85–89 (1999).

[20] J. W. G. Thomason, "The ISIS spallation neutron and muon source—The first thirty-three years," Nucl. Instrum. Methods Phys. Res., Sect. A **917**, 61–67 (2019).

[21] S. Imberti, W. Kockelmann, M. Celli, F. Grazzi, M. Zoppi, A. Botti, A. Sodo *et al.*, "Neutron diffractometer INES for quantitative phase analysis of archaeological objects," Meas. Sci. Technol. **19**(3), 034003 (2008).

[22] A. Pietropaolo, G. Festa, F. Grazzi, E. Barzagli, A. Scherillo, E. M. Schooneveld, and F. Civita, "A multitask neutron beam line for spallation neutron sources," Europhys. Lett. **95**(4), 48007 (2011).

[23] A. Fedrigo, D. Raspino, F. Grazzi, and A. Scherillo, "An integrated approach between neutron diffraction and elemental imaging through neutron resonance transmission imaging: Preliminary results on Chinese bimetallic sword fragments," J. Anal. At. Spectrom. **34**(12), 2420–2427 (2019).

[24] H. Postma, M. Blaauw, P. Bode, P. Mutti, F. Corvi, and P. Siegler, "Neutron-resonance capture analysis of materials," J. Radioanal. Nucl. Chem. **248**(1), 115–120 (2001).

[25] National Institute of Standards and Technology, https://www.nist.gov/laboratories/tools-instruments/instrumental-neutron-activation-analysis-inaa.

[26] M. Mocko, G. Muhrer, and F. Tovesson, "Advantages and limitations of nuclear physics experiments at an ISIS-class spallation neutron source," Nucl. Instrum. Methods Phys. Res., Sect. A **589**(3), 455–464 (2008).

[27] See https://www.ortec-online.com/ for Online catalogue.

[28] A. Sood, "Recent developments for MCNP6," Report No. LA-UR-09-1056, 2009.

[29] See https://www.armi.com/en/mbh-now-armi-mbh for Online catalogue.

[30] See https://www.techlab.fr/ for Online catalogue.

[31] M. Orioli, "Pastoralism and nomadism in South-West China: A brief survey of the archaeological evidence," in *The Archaeology of the Steppes: Methods and Strategies: Papers from the International Symposium Held in Naples 9–12 November 1992* (Istituto Universitario Orientale, 1994), pp. 87–108 .

[32] K. S. Krane and D. Halliday, *Introductory Nuclear Physics* 3rd edition (Wiley, 1987).

[33] S. Y. F. Chu *et al.*, The Lund/LBNL Nuclear Data Search, http://nucleardata.nuclear.lu.se/toi/.

[34] M. B. Chadwick *et al.*, "ENDF/B-VII.1: Nuclear data for science and technology: Cross sections, covariances, fission product yields and decay data," Nucl. Data Sheets **112**, 2887 (2011).

[35]A. Muraro *et al.*, "Performance of the high-efficiency thermal neutron BAND-GEM detector," Prog. Theor. Exp. Phys. **2018**(2), 023H01.
[36]D. Chiesa *et al.*, "Measurement of the neutron flux at spallation sources using multi-foil activation," Nucl. Instrum. Methods Phys. Res., Sect. A **902**, 14–24 (2018).
[37]M. S. Murty, K. Siddappa, and J. Rama Rao, "Capture cross sections of intermediate neutrons," J. Phys. Soc. Jpn. **35**(1), 8–11 (1973).
[38]B. H. Toby, "Rietveld refinement," in *International Tables for Crystallography* (IUCr Series, 2019), Vol. H, Chap. 4.7, pp. 465–472.